AIAA JOURNAL
Vol. 44, No. 6, June 2006

Parameterization of Temporal Structure in the Single-Dielectric-Barrier Aerodynamic Plasma Actuator

C. L. Enloe,* T. E. McLaughlin,† and G. I. Font‡
U.S. Air Force Academy, Colorado 80840
and
J. W. Baughn§
University of California, Davis, Davis, California 95616

We present the results of two measurements that describe the interaction of an aerodynamic plasma actuator (a dielectric barrier discharge plasma in which an asymmetric arrangement of electrodes leads to momentum coupling into neutral air) with the surrounding atmosphere. We show that the presence of oxygen in the Earth's atmosphere plays a substantial role in the efficiency of the actuator. We measure the time-resolved neutral air density in the vicinity of the actuator using a laser beam probe. We show that the effect of the actuator is to establish a region of increased neutral density in the vicinity of its exposed electrode's edge, and we show that the actuator couples directed momentum into the air by pulling air up this density gradient, against the corresponding pressure, and releasing it in the downstream direction when the plasma quenches, replacing it with air from the volume above the actuator. These measurements harmonize previously contradictory measurements of the actuator's behavior.

Nomenclature

ds	=	element of laser beam path
K	=	proportionality constant between neutral density and change in index of refraction
L	=	moment arm between the actuator and the detector face
m	=	mass
n	=	neutral air density
n_0	=	ambient neutral air density
$\tilde{n}$	=	index of refraction
$\tilde{n}_0$	=	ambient index of refraction
P	=	momentum
p	=	pressure
t	=	time
V_{app}	=	voltage applied to the plasma actuator
V_{out}	=	output signal from the position-sensitive detector circuit
w	=	width of plasma actuator
x	=	chordwise distance, origin at electrode edge
y	=	spanwise distance
z	=	height above plasma actuator
δy	=	linear deflection of laser beam across the detector face
$\delta\phi$	=	angular deflection of laser beam
τ	=	period of applied voltage waveform

I. Introduction

THE single-dielectric-barrier aerodynamic plasma actuator, a dielectric barrier discharge plasma in which an asymmetric arrangement of electrodes (one exposed, one encapsulated) leads to momentum coupling into neutral air,[1,2] has shown substantial promise as an aerodynamic flow control device combining the desirable attributes of high control authority, high bandwidth, electrical efficiency, and simplicity of construction (no moving parts).[3–15] At the U.S. Air Force Academy, in addition to investigating applications of this device in numerous settings, our approach includes experimental, theoretical, and computational studies of the physics of the device and of its interaction with the atmosphere, the goal of these studies being to optimize the construction and operation of the actuator.

In this paper, we present the results of two sets of measurements of the actuator's behavior, one in which we control the composition of the surrounding atmosphere in which the device operates, and one in which we probe the response of the atmosphere on the timescale of the ac high-voltage waveform applied to the actuator. The latter measurements, in particular, harmonize other observations of the actuator's behavior that heretofore have appeared to be contradictory and lead to important insights into the basic nature of the actuator's operation.

II. Fundamental Aspects of the Actuator's Operation

To understand the significance of the new measurements presented here, it is useful to review several aspects of the actuator's behavior that have been discovered to date. First and foremost, it is vital to realize that the plasma actuator is a form of dielectric barrier discharge, a device that is well known in the literature,[16–30] although the particular "surface discharge" mode that composes the actuator[1,2,16,25] has not been studied nearly to the degree of the discharge between parallel plate electrodes. The elements of the surface discharge configuration are shown schematically in Fig. 1. This figure is a notional drawing; typically, the thickness of the actuator electrodes is much smaller (0.08 mm) than their widths (that is, their chordwise dimensions), which are in the range of 3–6 mm for the exposed electrode and 6–25 mm for the encapsulated electrode. The chordwise extent of the plasma varies over the discharge cycle, but typically does not exceed that of the encapsulated electrode by more than a few mm. The plasma extends 1–2 mm above the surface of the dielectric material. In our investigations, the thickness of the dielectric has varied widely from 0.1 to 3 mm.

As a dielectric barrier discharge, the actuator plasma has structure on multiple timescales. The plasma exists as a series of microdischarges on the timescale of tens of nanoseconds.[16,17,20,22,26,28–30] These microdischarges can be seen as individual events in Fig. 2, a time history of light emitted from the actuator surface. Because

Presented as Paper 2005-0564 at the Aerospace Sciences Meeting, Reno, NV, 10–13 January 2005; received 25 February 2005; revision received 28 July 2005; accepted for publication 5 August 2005.

*Professor, HQ USAFA/DFP, Department of Physics. Senior Member, AIAA.
†Director, HQ USAFA/DFAN, Aeronautics Research Center, Department of Aeronautics. Associate Fellow AIAA.
‡Associate Professor, HQ USAFA/DFP, Department of Physics. Member AIAA.
§Professor, Department of Mechanical and Aeronautical Engineering, Member AIAA.

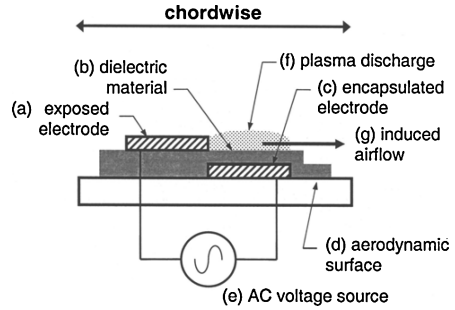

Fig. 1 Schematic representation of the "surface mode" dielectric barrier discharge that composes the aerodynamic plasma actuator.

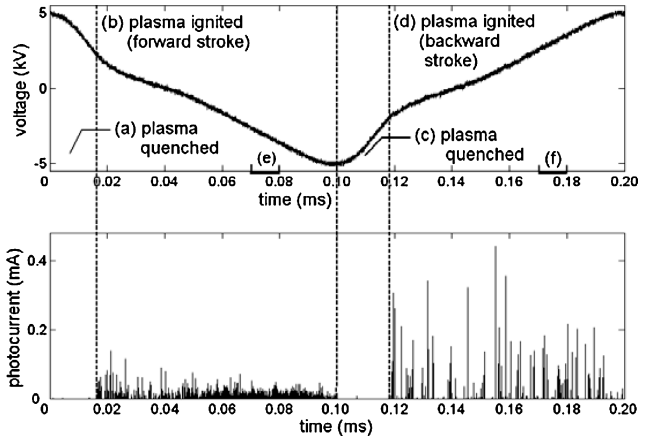

Fig. 2 Individual microdischarges are evident in the light emission from the plasma actuator.[16]

these microdischarges deposit charge on the dielectric surface that tends to reduce the applied electric field at that location, the plasma is self-limiting, and the microdischarge events naturally spread relatively uniformly along the length of the electrodes (as opposed to a typical spark in atmospheric-pressure air, which tends to pinch into a narrow column avalanche discharge due to the electromagnetic forces in play). This self-limiting behavior also shuts down the discharge on the macro scale, so that it is necessary to continually change the voltage applied to the electrodes to sustain the plasma. We have shown that the overall envelope of the discharge proceeds in six well-defined steps for every cycle of the ac voltage applied to the device: ignition, expansion, and quenching of the "forward stroke" (during which electrons are drawn from the exposed electrode to the dielectric surface) followed by ignition, expansion, and quenching of the "backward stroke" (during which electrons return from the dielectric surface).[16] This behavior can readily be seen in the optical emissions from the plasma, shown in Fig. 3. Our new measurements of the actuator's interaction with the air indicate that the quenching phase of the cycle is as important to the actuator's coupling momentum to the neutral air as those phases in which the plasma is present.

Second, the spatial and temporal structures of the plasma during the forward and backward strokes of the discharge are not the same. We have shown that the forward stroke is much more macroscopically diffuse (thus interacting with a larger volume of atmosphere) than the backward stroke.[1,16] We have shown (Fig. 4) that the actuator is more effective when a larger fraction of the ac cycle is spent in the forward vs the backward stroke.[1] These observations are consistent with the new measurements presented here.

Third, there are two sets of observations that until this time seemed to give contradictory views of how the plasma interacted with the surrounding air. We have shown that the force produced by the actuator, for essentially identical overall discharge characteristics in the plasma, varies considerably with the edge radius of the exposed electrode.[2] This variation is shown in Fig. 5. This indicated that the

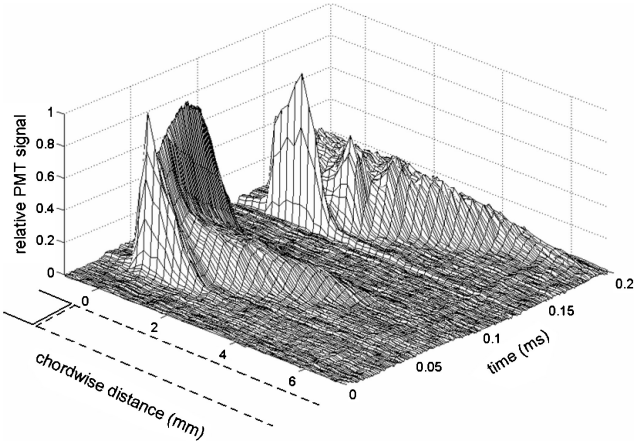

Fig. 3 Separate ignition, expansion, and quenching phases of the actuator's discharge cycle are evident in the light emission from the device.[2] The boundary between the exposed electrode (sketched using a solid line) and the encapsulated electrode (dashed line) is at chordwise location $x = 0$.

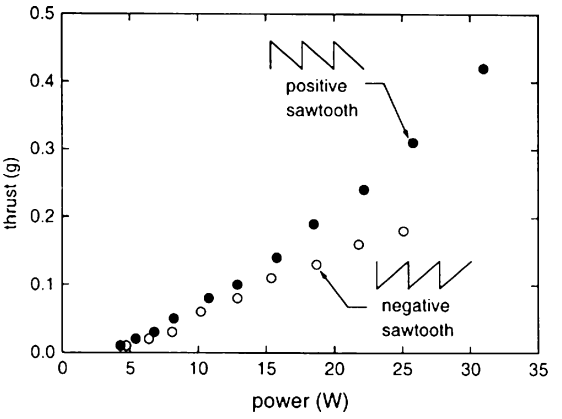

Fig. 4 Actuator is more effective when a larger fraction of the ac cycle is spent in the forward vs the backward stroke.[1]

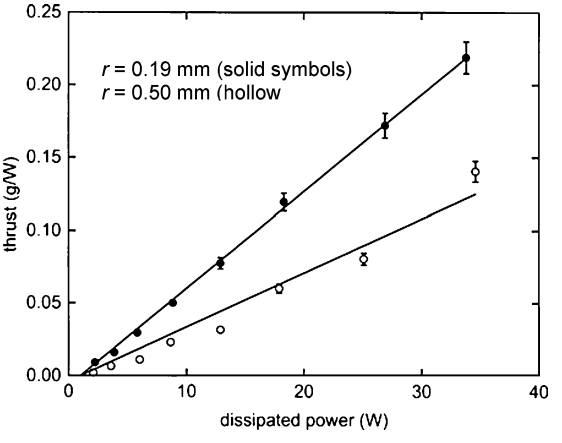

Fig. 5 Configuration of the exposed electrode edge has a substantial effect on the actuator's performance.[2]

high-electric-field region near the edge of the exposed electrode is the critical portion of the plasma, as far as its efficiency is concerned. Other data, however, pointed to the leading edge of the plasma expansion, downstream of the exposed electrode, as the critical region of the plasma. Specifically, we have shown that the expansion of the plasma over the dielectric surface (shown in Fig. 3) is limited to the extent of the encapsulated electrode, and furthermore that when the plasma reaches this physical limit, its efficiency of operation also plateaus, as seen in the data shown in Fig. 6, for the 8- and

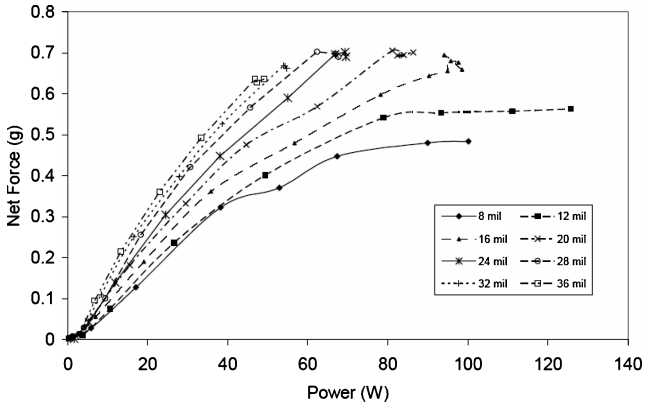

Fig. 6 Performance of the actuator plateaus when the extent of plasma is limited by the encapsulated electrode's width, for cases in which the plasma reaches the edge of the encapsulated electrode.[31]

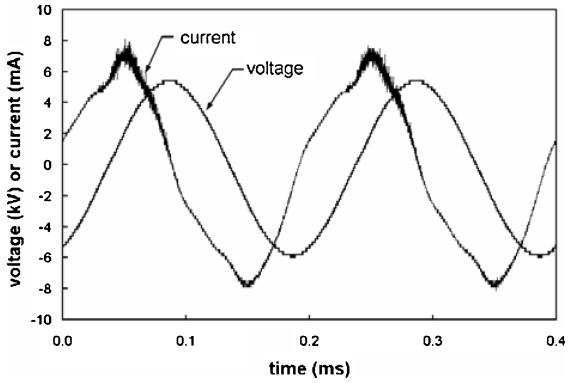

Fig. 7 Power dissipated by the actuator is calculated by integrating the product of the measured voltage across and the measured current through the actuator over an integral number of ac cycles.

12-mm-thick dielectrics.[31] (The effect is not seen in this configuration for thicker dielectric barriers, because the expansion speed of the plasma is determined in part by the capacitances in the actuator circuit.) The new data we present here harmonize these two effects in a comprehensive view of the actuator's interaction with the surrounding air.

We note that the data presented in the previous three figures depend on a crucial parameter of the actuator, the power dissipated by the device. We calculate this quantity from simultaneous measurements of the voltage applied to, and the current through, the actuator. Because the dielectric barrier discharge is composed of many individual microdischarge events, the instantaneous current through the device, and hence the instantaneous power it dissipates, is highly variable in time. Nonetheless, averaged over many ac cycles, the current is quite predictable, as shown in Fig. 7. We integrate the product of averaged, instantaneous current and instantaneous voltage over an integral number of ac cycles to calculate the power dissipated in the actuator. We note, further, as shown in Fig. 7, that a large fraction of the current through the device is displacement current through the capacitive elements of the device. Although displacement current is important from a systems design standpoint, since the power system must be able to supply it, only the current through the dissipative element in the circuit—the plasma—contributes to the power dissipation of the device.

Fourth, numerical modeling of the plasma appeared, until now, to be at odds with the observed behavior of the device. Figure 8 shows the results of a particle-in-cell simulation of a single microdischarge event in nitrogen gas, on the forward stroke of the discharge.[32] In this simulation, a voltage is applied between the exposed and the encapsulated electrodes. A seed population of electrons is introduced near the edge of the exposed electrode, and as the electrons accelerate in the electric field, they ionize the background gas. The contribution

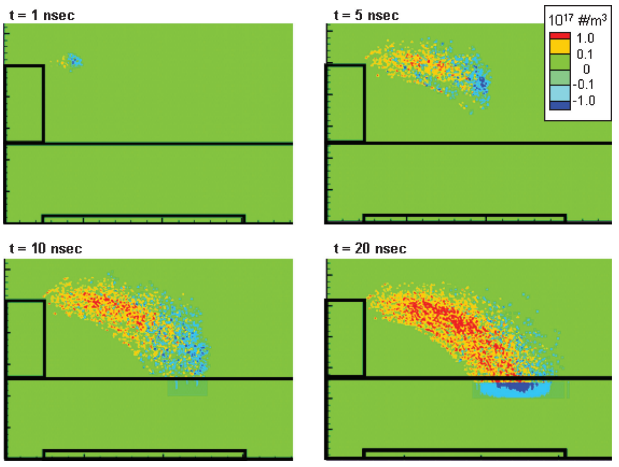

Fig. 8 Results of a particle-in-cell simulation of a single microdischarge event.[32] Because the quantity shown here is net density of charged particles, red indicates an excess of ions in a given region and blue shows an excess of electrons.

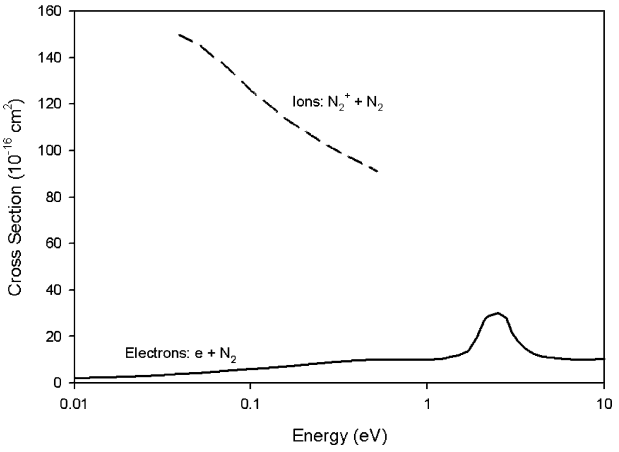

Fig. 9 Momentum exchange cross sections for ions and electrons in neutral air.

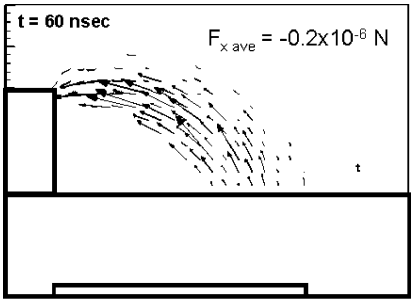

Fig. 10 Calculated force on the plasma ions due to the electric field, which is the force felt by the neutrals due to collisions.[32]

of the free charges represented by the electrons and the ions is taken into account in recalculating the electric field at each time step in the simulation. As the simulation shows, portions of the volume become either electron- or ion-rich as the electrons are drawn toward the dielectric surface. Ions feel a force toward the exposed electrode, although they do not experience the motion that the electrons do, because the ions have a strong momentum-exchange interaction with the background neutrals. Cross sections for the predominant ion-neutral momentum exchange interactions are compared in Fig. 9 with the corresponding interaction for electrons,[33–35] and it is on the basis of these cross sections that we calculate the force on the neutral atmosphere by the plasma, as shown in Fig. 10. The heretofore contradictory result is that the net force on the neutral air is in the

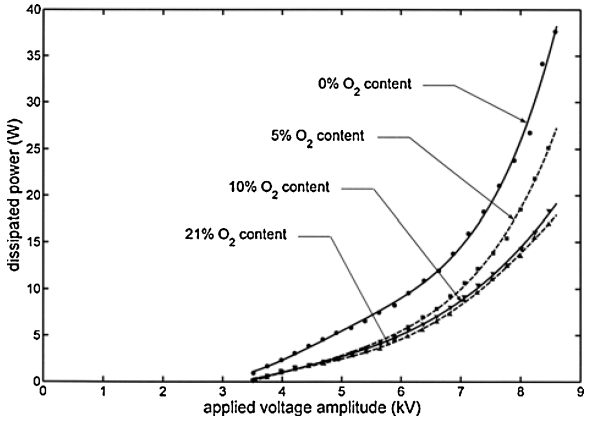

Fig. 11 Oxygen content of the air only mildly affects the actuator's discharge properties.

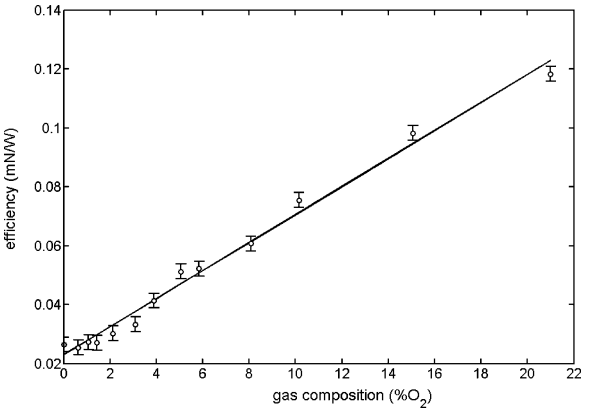

Fig. 12 Oxygen content of the air substantially affects the actuator's efficiency.

direction opposite to the net flow of the air observed in the laboratory. The results we present here explain this apparent contradiction.

III. Atmospheric Composition Effects

Our numerical simulations, as shown in Fig. 8, are for an electropositive plasma—that is, a plasma in which there is a population of massive, positive ions and light, negative electrons. We know, however, that the presence of oxygen in Earth's atmosphere also allows for the formation of a smaller, yet important, population of negative ions via attachment of electrons to the oxygen. To investigate whether this effect is important in our understanding of the operation of the plasma actuator, we operated the device in a controlled mixture of nitrogen and oxygen, covering the range from <0.1% O_2 to the natural 21% O_2 composition of air. We did this by placing the actuator in the 1.8-m-diam × 2-m-long space simulation chamber at the U.S. Air Force Academy. The chamber was evacuated using a mechanical roughing pump to a pressure of <100 mtorr, and then backfilled with pure N_2 to the ambient pressure at the Academy, 600 torr. Subsequently, a portion of the gas in the chamber was pumped out, and the chamber was vented to room air. By controlling the amount of gas removed at each step, we could gradually increase the oxygen content of the atmosphere in which the actuator was operated. When operating the actuator, we measured the voltage applied to the device using a high-voltage probe (Textronix Model P6015) while simultaneously measuring the current through the device with a self-integrating Rogowski coil (Pearson Electronics Model 150 current probe, rise time = 20 ns). Thus, we could calculate the power dissipated by the plasma over one ac cycle. We also measured the force produced by the airflow around the actuator, as we had in previous experiments.

The results showed that removing all of the oxygen from the atmosphere had a measurable effect on the gross discharge characteristics of the plasma, as indicated by the relationship between dissipated power and voltage shown in Fig. 11. Introducing oxygen into the system, however, rapidly mitigated this change, so that, as Fig. 11 shows, the gross discharge characteristics of the plasma with a 10% oxygen atmosphere and with a 21% oxygen atmosphere were virtually identical. The efficiency of the actuator, however, showed substantial variation over this range. Figure 12 shows the efficiency of the actuator, as quantified by the measured force per unit of power dissipated by the device, as a function of the composition of the atmosphere in which it operates. The efficiency of the device is directly correlated with the fraction of oxygen in the atmosphere. Clearly, the electronic properties of oxygen have a major impact on the operation of the aerodynamic plasma actuator.

IV. Time-Resolved Measurements of the Actuator's Interaction with the Air

There have been a considerable number of attempts to understand the interaction of the actuator plasma with the surrounding air: this is, after all, the crux of any understanding of the device

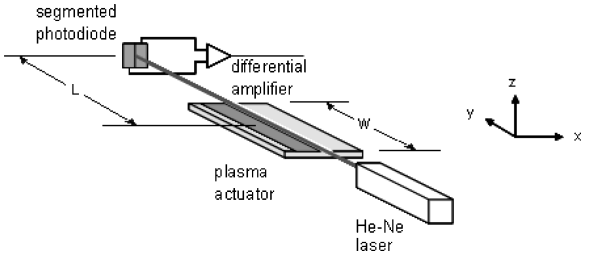

Fig. 13 Laser deflection technique measures density by probing index of refraction gradients in the air.

overall. Until now, however, these explanations have been somewhat speculative due to a lack of measurements of the behavior of the air on the timescales of the temporal structure of the plasma. In this paper, we present measurements of that behavior using a straightforward, nonintrusive optical technique. This technique has considerable successful history in the literature,[35–38] does not perturb the system being probed, is easily calibrated, and is reliable enough to be used even in the teaching laboratory.[39]

A. Laser Deflection Probe

The measurement technique we used to observe the air in the vicinity of the plasma actuator on the timescales of the envelope of the discharge relies on the fact that, in any inhomogeneous medium, light refracts through gradients in the index of refraction. For neutral air, the deviation of the index of refraction $\delta\tilde{n}$ from the vacuum value (which is 1) is linearly proportion to the neutral density n and is given by[37]

$$\delta\tilde{n} = (\tilde{n}_0 - 1)(n/n_0) = Kn \tag{1}$$

where n_0 is the ambient density of the neutral air and $\tilde{n}_0$ is the corresponding index of refraction at this density. The constant K is independent of n_0, but can be readily calculated from the density of air at standard temperature and pressure as $n_0 = 2.69 \times 10^{25}$ m^{-3} and the index of refraction at is $\tilde{n}_0 = 1.000276$,[35] so that $K = 1.03 \times 10^{-29}$ m^3. To implement this principle as a probe of the air density, we pass a beam of laser light above the plasma actuator, in the manner shown in Fig. 13. The beam falls on a bifurcated photodiode (essentially two photodiodes on a single substrate, with a micrometer-width separation between them), the outputs of which are input to a differential amplifier circuit. With the beam centered between the two halves of the detector, the differential amplifier signal is zero, but if the beam is deflected perpendicular to the line of separation, then the amplifier output will be a nonzero value, positive or negative depending on the direction of the deflection. The aspect ratio of the detector is large enough so that the beam can deflect parallel to the line of separation without falling outside the active area of the detector; therefore, the device is sensitive to gradients in only one direction. The output voltage V_{out}

of the amplifier circuit depends on the linear deflection of the beam at its location, which in turn depends on the angular deflection $\delta\phi$ of the beam from its unperturbed path. This quantity is given by[37]

$$\delta\phi = (1/\tilde{n}_0)\int_{\text{path}} \mathrm{d}s\,\Delta_\perp \tilde{n} \tag{2}$$

where s is the path of the laser; Eq. (2) indicates that the beam is deflected by gradients perpendicular to its path. Because the deflections of the beam are small, s is simply a straight-line path in the $\hat{y}$ direction, of length w, the width of the actuator. Because the deflection $\delta\phi$ is small, we can apply the small-angle approximation $\delta\phi \approx \delta y/L$, where δy is the deflection of the beam across the face of the detector, and L is the moment arm from the center of the actuator to the detector's location. Finally, because $1/\tilde{n}_0 \approx 1$, we can write

$$\frac{\delta y}{L} = w\left\langle \frac{\partial \tilde{n}}{\partial x} \right\rangle \tag{3}$$

Using Eq. (1), we find that the perpendicular gradient in the density can be found from

$$\left\langle \frac{\partial n}{\partial x} \right\rangle = \frac{\delta y}{wLK} \tag{4}$$

The relationship between the output voltage V_{out} of the detector and the deflection of δy the beam can be determined by moving the beam over a series of known distances (in the absence of the actuator). Thus, with the gradient of the density known, the variation from ambient density, $\delta n(x,t)$, can be determined by scanning the laser in the x direction for a fixed location in z and then integrating the results:

$$\delta n(x,t) = \int \mathrm{d}x \frac{\partial n(t)}{\partial x} \tag{5}$$

assuming that the integration starts in an unperturbed region of space. This process can be repeated at different z-axis locations to generate a two-dimensional map of the air density as a function of time in the region above the plasma actuator. The laser deflection technique is inherently fast and in practice is limited by the speed of the electronics involved. For our experiment, the bandwidth of the measurement is approximately 100 kHz.

Implementing the laser deflection technique using a segmented photodiode, as we have done here, introduces one instrumental limitation into our measurements—due to the small active area of the detector (1 mm in the x direction $\times 5$ mm in the z direction), and the fact that the analysis assumes a Gaussian beam profile falling on the detector, we are unable to probe the region of strong gradients within 1 mm of the dielectric surface—we find that the beam deflects in the z direction outside the detector's active area. A preferred (albeit more expensive) implementation is to use a true centroid detector (available with active areas of several cm^2) to measure the deflections, which would eliminate this limitation. We hope to construct such a system in the future; nonetheless, the data presented here shed considerable light on the operation of the plasma actuator.

B. Results of the Laser Deflection Measurements

We present here the density as a function of time for the case of a plasma actuator operated with a 5-kHz sine-wave high-voltage waveform at a voltage amplitude of 8 kV. Fig. 14 shows the net change in density as a fraction of the ambient density over 0.4 ms (that is, two complete ac cycles) at a height of 1 mm above the aerodynamic surface, for distances 5 mm upstream and 10 mm downstream of the electrode edge. The data reveal a substantial density buildup (approximately 2% of the ambient density) near the edge of the exposed electrode. The data also show that the particles in this density peak are taken from downstream of the electrode: from the region in which the plasma interacts with the neutral air. This observation harmonizes the apparent discrepancy between the direction of the force on the ions and the direction of the momentum coupling

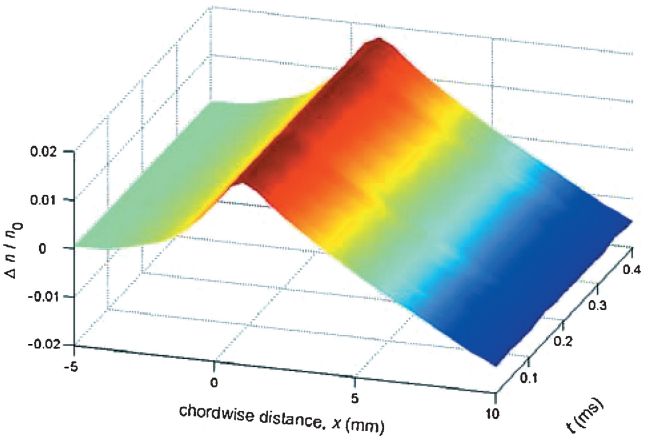

Fig. 14 Actuator produces a dc average density increase in the vicinity of the exposed electrode's edge, shown here at a height of 1 mm above the surface.

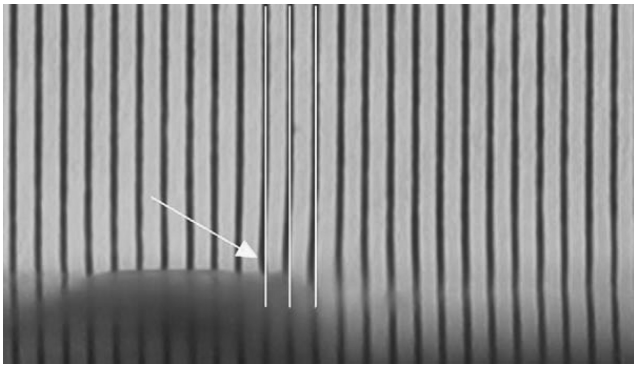

Fig. 15 Pressurization of the air near the edge of the actuator is substantial enough that it can be viewed by the unaided eye and appears as a distortion of the background pattern placed behind the actuator.

to the air, namely, that the force on the ions due to the electric field in the plasma is upstream, toward the edge of the exposed electrode, whereas the net momentum coupling to the air is in the downstream direction, away from the electrode edge. Simply put, the action of the actuator is to pressurize the region near the electrode edge and to establish a favorable pressure gradient so that the negative gradient of the pressure $-\nabla p$ is in the downstream direction. The existence of this favorable pressure profile is substantial enough so that it can be viewed by the unaided eye; although we do not derive quantitative information from these observations as we do from the laser deflection measurements, we offer Fig. 15 (an edge-on photograph of the actuator against a uniform striped background) as an indication of the magnitude of this pressurization effect, which is seen as a distortion of the background pattern in the figure.

Of even more significance is the manner in which the actuator not only maintains this density gradient (and the corresponding pressure), but accesses this structure to impart momentum to the flow. Careful observation of the data in Fig. 14 reveals a periodic structure in time in the density profile. Although these variations can be difficult to resolve against the overall density structure, their nature is revealed when we subtract the average value of the density at each point in space from the particular value at a given time. These data are best viewed as two-dimensional slices at different times, that is, as movie frames. A set of these snapshots is shown, over one ac cycle of the discharge, in the extensive Fig. 16. The top graph in each frame of Fig. 16 shows the average light emission from the plasma, so that by following this graph we can determine whether the plasma is ignited or quenched at any particular time. The middle graph shows the voltage applied between the electrodes of the actuator. We emphasize that this is not the voltage seen across the plasma, due to the reactive nature of the circuit. Nevertheless, it is a useful

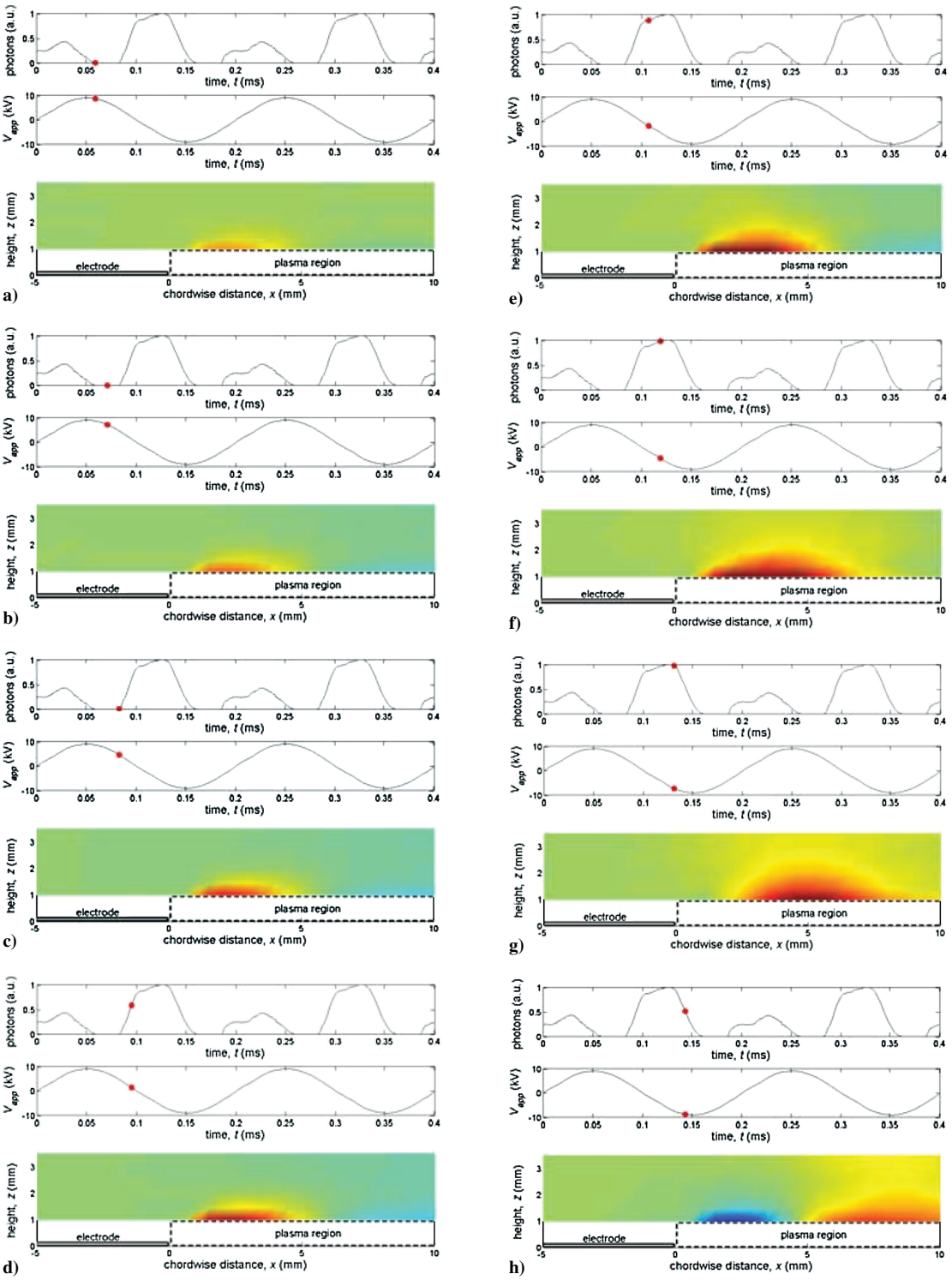

Fig. 16 AC variation in the neutral density reveals the action of the plasma actuator. For each frame, the top trace shows light emission (in arbitrary units), whereas the middle trace shows the voltage applied to the actuator (±10 kV full scale). The lower portion of each frame shows density variations over a 15 × 3.5 mm cross section of the actuator. Full-scale density variation is 0.08% of ambient in the positive (red) or negative (blue) direction.

measurement, because we know that when the applied voltage is negative-going, we are in the forward stoke of the discharge, and in the backward stroke when the applied voltage is positive-going. The bottom graph in each frame shows the density variation from the average in two spatial dimensions. In these figures, the red end of the color spectrum represents positive density excursions above the local time-averaged value shown in Fig. 14, whereas the blue end of the spectrum shows reduced densities relative to the average. Full scale excursions in Fig. 16 are 0.08% variation from the ambient density.

We begin our observations in Fig. 16a, at the extinction phase of the plasma after the backward stroke. As we see in Fig. 16a, there is a small density increase near the electrode edge left over from the previous cycle. This density perturbation remains during the quenching period (and even increases slightly, which we take to be the result of inertia in the moving fluid) until the forward stroke of the discharge initiates in Fig. 16c. At this point, the density increase near the electrode edge begins to steepen, and continues to do so as long as the time derivative of the applied voltage dV_{app}/dt remains approximately constant, that is, until Fig. 16f. Significantly,

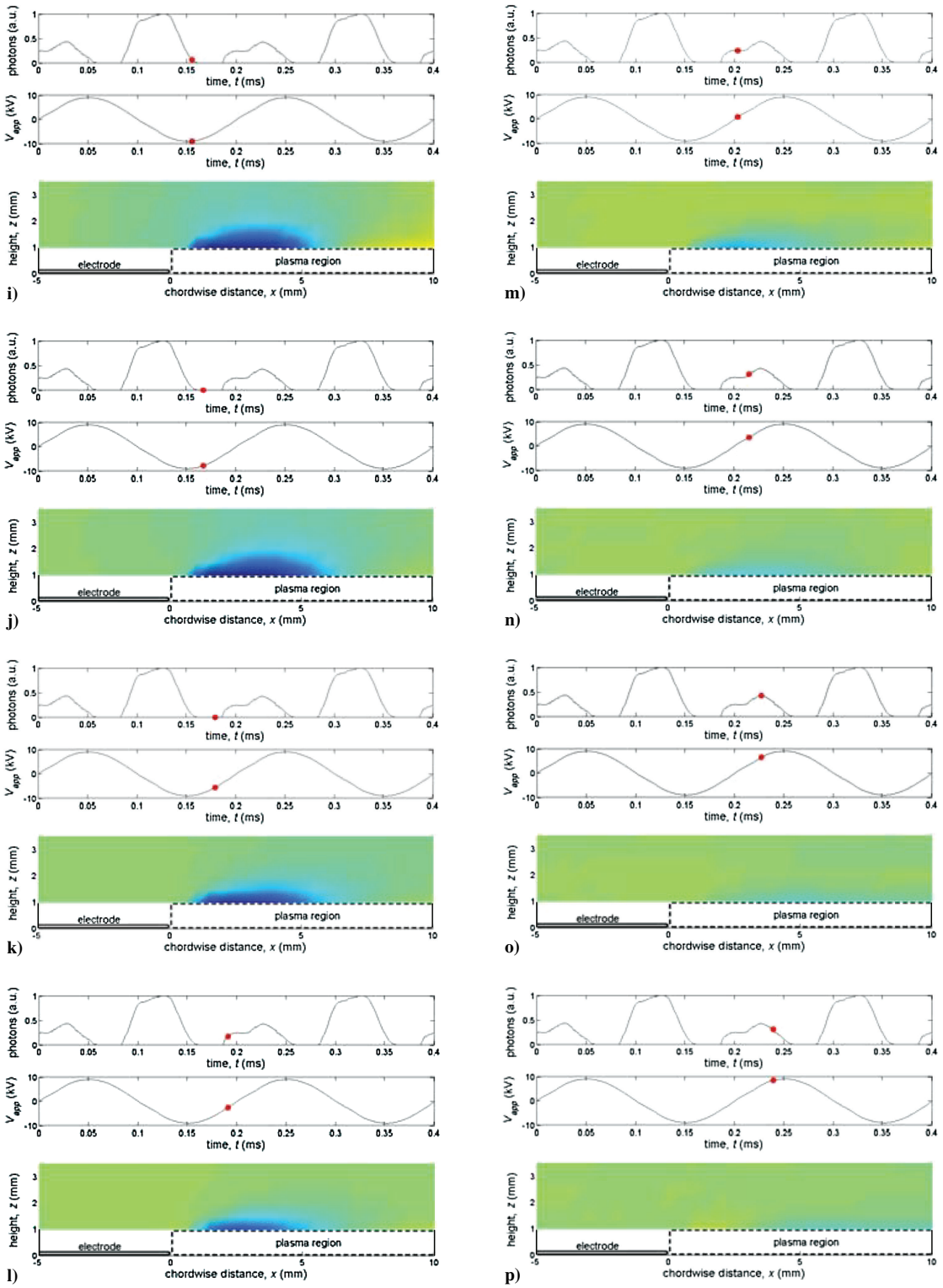

Fig. 16 AC variation in the neutral density reveals the action of the plasma actuator. For each frame, the top trace shows light emission (in arbitrary units), whereas the middle trace shows the voltage applied to the actuator (±10 kV full scale). The lower portion of each frame shows density variations over a 15 × 3.5 mm cross section of the actuator. Full-scale density variation is 0.08% of ambient in the positive (red) or negative (blue) direction (continued).

although the density increases, the location of the density peak does not move substantially until the magnitude of $\mathrm{d}V_{\mathrm{app}}/\mathrm{d}t$ decreases. Also, we see a density decrease downstream of the electrode edge during this buildup, indicating that the plasma is scooping air from downstream into the region near the electrode edge.

When the magnitude of $\mathrm{d}V_{\mathrm{app}}/\mathrm{d}t$ begins to drop off substantially, we are no longer able to sustain the voltage drop across the plasma itself: the electric field due to the electrons deposited on the dielectric surface cancels the applied field. We see the effect on the discharge, in that the intensity of the light emission falls off, indicating that the plasma production is no longer able to keep up with the recombination. As the electric field and the charged particle density simultaneously decrease, so does the electric force per unit volume on the air, and as a consequence, the density buildup near the edge is no longer sustainable, resulting in dramatic relaxation of the density in the downstream direction (recall that the overall $-\nabla p$ force is

in this direction), and subsequent rarefaction behind it, as shown in Figs. 16g–16i. This rarefaction then decays during the remaining portions of the ac cycle (Figs. 16j–16p), including both the quenching phase following the forward stroke and the backward stroke of the discharge. We note, from the spatial uniformity of the rarefaction as it shrinks, that the air filling in this density depression appears to be coming from the region above the actuator. (This is consistent with flow visualizations that have been made of the bulk airflow near the actuator, which indicate that air is diverted down from the region above the actuator, to be ejected in the downstream direction.) Only in the later stages of the backward stroke does a small density increase appear near the edge of the exposed electrode.

We readily state that with these measurements we are not measuring fluid velocities directly, but rather are inferring them from frame-to-frame variations in spatial densities. Nonetheless, these observations are consistent with the following picture of the actuator's operation: Once the actuator establishes the pressurization near the edge of the exposed electrode, it subsequently displaces air upstream against that density gradient (that is, against the pressure), releasing it downstream when the plasma quenches. We also note that these direct measurements of the density perturbations as a function of time are consistent with our measurements of the acoustic signature of the actuator, which significantly includes a strong frequency component at twice the frequency of the ac waveform driving the actuator.[40]

Of course, it is reasonable to ask whether the phenomenon presented here is sufficient to account for the macroscopic momentum transfer we observe with the plasma actuator. The thrust F_{exp} that we observe experimentally with the actuator used in this setup, with the operating parameters used for these measurements, is $F_{\text{exp}} = 6.7$ mN. By Newton's law, this force is simply the time rate of change $\Delta P/\Delta t$ of momentum imparted to the surrounding air, so that if we attribute this force to imparting a velocity Δv to a mass m of air over a time period τ that is the period of the AC driving waveform applied to the actuator, we have

$$F = \Delta p/\Delta t = m\Delta v/\tau \tag{6}$$

For our actuator, the period τ is very well defined, $\tau = 0.2$ ms. The velocity imparted to the pulse of air ejected from the interaction region is relatively easy to estimate; by observing the frames in Figs. 16g–16i, we see the pulse moving a distance of approximately 5 mm in a time of 0.03 ms, for a velocity of $\Delta v = 167$ m/s. The most difficult quantity to establish is the mass of air involved in the momentum transfer, because the laser cannot probe the region where the plasma exists. Nonetheless, we can bound this value as follows: We note that the density perturbation involved in the pulse is approximately 0.08% of the ambient air density, and that the pulse leaves a void of approximately the same magnitude in its wake, so we are dealing with a perturbation of approximately 0.15% of the ambient density, which equates to a mass density of 1.6×10^{-3} kg/m^3. We estimate the volume of the perturbed region to be a volume of 4 to 5 mm in each cross-sectional dimension by 23 cm, the spanwise width of the actuator. Using these dimensions, we estimate the mass m involved in each pulse to be between 6×10^{-9} and 9×10^{-9} kg. Using these values in Eq. (5), we predict the thrust due to the observed, periodic mass ejections from the actuator's interaction region to be 5.0 mN $< F <$ 7.6 mN. That is, the phenomenon presented here is entirely sufficient to account for the observed macroscopic behavior of the plasma actuator.

C. Implications of the Laser Deflection Measurements

We have already discussed, in the preceding section, how the time-dependent density measurements made using the laser deflection technique are consistent with other measurements that have been made on the aerodynamic plasma actuator. These measurements, however, point toward a more global issue: the density structures revealed by this technique cannot be properly understood without clearly understanding the nature of the plasma/neutral fluid interaction on timescales where the fluid inertia plays a major role. For example, we previously understood that choosing an ac waveform that kept the plasma ignited for a substantial fraction of the time was important to optimizing its operation, because without the plasma, there is no force. These results, however, indicate that the quenching period is equally important to the actuator's operation, and that in order for the actuator to operate effectively, the plasma must remain quenched for a period of time that is long enough to allow the mass ejection to occur. The implications of this understanding have practical consequences: although we know that it is possible to reduce the mass of some of our components (desirable, of course, for flight applications) by going to higher frequencies, these results predict that pushing operation of the actuator to higher frequencies is at odds with the reaction time of the neutral fluid to the time-varying force from the plasma. In fact, this is what we observe. Figure 17 shows that the thrust (that is, the momentum transfer) from our actuators decreases with increasing frequency of the driving waveform when we hold the power dissipated by the actuator constant. Other users have reported an increase in actuator effectiveness as frequency of operation is increased into the range of tens of kilohertz. We also observe this, if we keep the amplitude of the applied voltage constant (also shown in Fig. 17). This behavior, however, is misleading. From a circuit perspective, the plasma actuator is a complex set of capacitances with one resistive element, the plasma itself, all of which evolve over the period of the driving waveform,[1,41] but in its simplest form, the actuator may be seen as a resistor (the plasma, which bridges the exposed electrode and the dielectric surface) and a capacitor (which is formed between the "effective electrode" at the dielectric surface, where charge accumulates, and the encapsulated electrode.) As the frequency of the driver increases, the impedance of the capacitor decreases, and a larger fraction of the voltage across the capacitive/resistive divider appears across the plasma. (The voltage across the plasma is a difficult measurement to make, and estimating this value based on the agreement between numerical models and measurable quantities in the circuit is a topic of ongoing research.[41]) When we measure the power dissipated by the actuator, however, we see that the efficiency of the device (force per unit power) is approximately the same whether one holds power or voltage constant (as shown in Fig. 18), and if anything falls off at higher frequency in the constant-voltage case. Although in terms of overall system parameters, it may be desirable to accept somewhat reduced efficiency as the price for reduced mass, the principle still holds: Fluid inertia effects are fundamental to the operation of the aerodynamic plasma actuator and must be considered in any complete analysis of its operation.

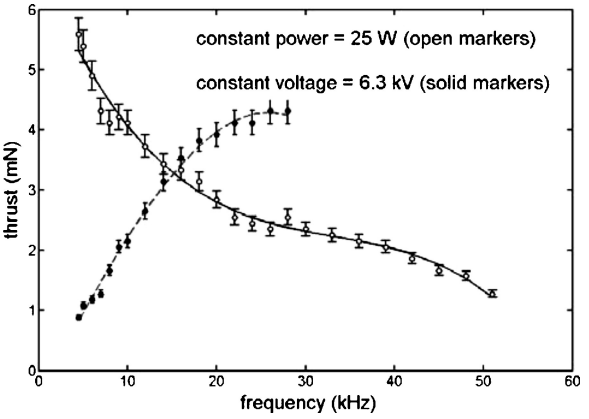

Fig. 17 Thrust (momentum coupling) from the actuator as a function of frequency.

Finally, although in practical terms we do not anticipate operating in an oxygen-free environment, including the particular properties of oxygen is apparently important to completing the picture we have of the actuator's workings. At this point, we can say that the presence of negative oxygen ions, which would tend to accumulate near the electrode edge during the "backward stroke" of the discharge, is not inconsistent with the premise of the actuator's operation: namely, any effect that tends to sharpen the dc density gradient near the electrode edge by increasing the time-averaged force directed toward the

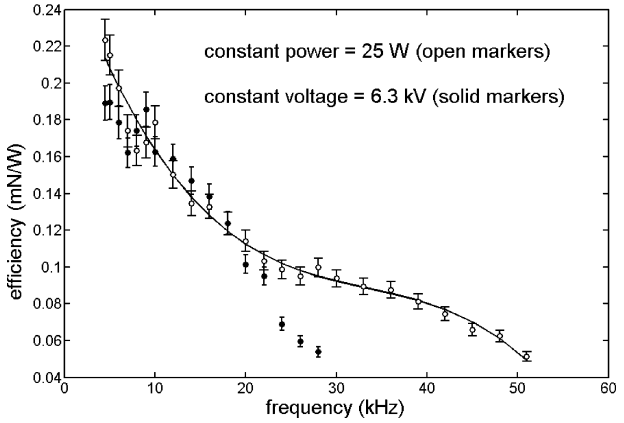

Fig. 18 Efficiency of momentum coupling from the actuator as a function of frequency.

edge tends to increase the performance of the actuator. In short, fruitful areas of study remain, the importance of which is indicated by the new results presented in this paper.

V. Conclusions

The description of the aerodynamic plasma actuator's interaction with the neutral air indicated by the density measurements made here—namely, the pressurization of the region near the exposed electrode edge, followed by periodic releases of "scoops" of air loaded by the plasma into this region—is consistent with every measurement we have made of the device to date, and in fact harmonizes measurements that appeared to point to different explanations of the actuator's workings. In particular, this description explains how the effect of ions moving upstream toward the exposed electrode can result in a new momentum transfer in the downstream direction. It explains the importance of the electric field structure in the region near the electrode edge: the larger the E field, the larger the force in that region, and the larger the density perturbation that can be maintained. At the same time, it explains the limitation of the actuator's effectiveness when the volume of air from which it can load the density perturbation is limited by the extent of the encapsulated electrode. This work points to the importance of understanding the interplay between the time-varying plasma structure and the dynamics of the neutral fluid on the kilohertz timescales in optimizing the effectiveness of the aerodynamic plasma actuator.

Acknowledgments

The authors gratefully acknowledge the support of the Air Force Office of Scientific Research, John Schmisseur, Program Manager, for the work presented here.

References

[1]Enloe, C. L., McLaughlin, T. E., VanDyken, R. D., Kachner, K. D., Jumper, E. J., and Corke, T. C., "Mechanisms and Responses of a Single Dielectric Barrier Plasma Actuator: Plasma Morphology," *AIAA Journal*, Vol. 42, No. 3, 2004, pp. 589–594.

[2]Enloe, C. L., McLaughlin, T. E., VanDyken, R. D., Kachner, K. D., Jumper, E. J., Corke, T. C., Post, M., and Haddad, O., "Mechanisms and Responses of a Single Dielectric Barrier Plasma Actuator: Geometric Effects," *AIAA Journal*, Vol. 42, No. 3, 2004, pp. 595–604.

[3]McLaughlin, T., Munska, M., Vaeth, J., Dauwalter, T, Goode, J., and Siegel, S., "Plasma-Based Actuators for Cylindrical Wake Vortex Control," AIAA Paper 2004-2129, June 2004.

[4]Corke, T., and He, C., "Plasma Flaps and Plasma Slats: An Application of Weakly-Ionized Plasma Actuators," AIAA Paper 2004-2127, June 2004.

[5]Post, M., and Corke, T., "Separation Control Using Plasma Actuators: Dynamic Stall Control on and Oscillating Airfoil," AIAA Paper 2004-2517, June 2004.

[6]Post, M., and Corke, T., "Separation Control Using Plasma Actuators—Stationary & Oscillating Airfoils," AIAA Paper 2004-841, Jan. 2004.

[7]Wilkinson, S., "Investigation of an Oscillating Surface Plasma for Turbulent Drag Reduction," AIAA Paper 2003-1023, Jan. 2003.

[8]Post, M., and Corke, T., "Separation Control on High Angle of Attack Airfoil Using Plasma Actuators," *AIAA Journal*, Vol. 42, No. 11, 2004, pp. 2177–2184.

[9]Ashpis, D., and Hultgren, L., "Demonstration of Separation Delay with Glow Discharge Plasma Actuators," AIAA Paper 2003-1025, Jan. 2003.

[10]List, J., Byerley, A., McLaughlin, T., and VanDyken, R., "Using Plasma Actuator Flaps to Control Laminar Separation on Turbine Blades in a Linear Cascade," AIAA Paper 2003-1026, Jan. 2003.

[11]Huang, J., Corke, T., and Thomas, F., "Plasma Actuators for Separation Control of Low Pressure Turbine Blades," AIAA Paper 2003-1027, Jan. 2003.

[12]Corke, T. C., Jumper, E. 1., Post, M. L., Orlov, D., and McLaughlin, T. E., "'Application of Weakly-Ionized Plasmas as Wing Flow-Control Devices," AIAA Paper 2002-0350, Jan. 2002.

[13]Roth, J. R., Sherman, D. M., and Wilkinson, S. P., "Electrohydrodynamic Flow Control with a Glow-Discharge Surface Plasma," *AIAA Journal*, Vol. 38, 2000, pp. 1166–1172.

[14]Corke, T. C., and Matlis, E., "Phased Plasma Arrays for Unsteady Flow Control," AIAA Paper 2000-2323, Jan. 2000.

[15]Roth, J. R., Sherman, D. M., and Wilkinson, S. P., "Boundary Layer Flow Control with a One Atmosphere Uniform Glow Discharge Surface Plasma," AIAA Paper 98-0328, Jan. 1998.

[16]Enloe, C. L., McLaughlin, T. E., VanDyken, R. D., and Fischer, J. R., "Plasma Structure in the Aerodynamic Plasma Actuator," AIAA Paper 2004-844, Jan. 2004.

[17]Kogelschatz, U., "Filamentary, Patterned, and Diffuse Barrier Discharges," *IEEE Transactions on Plasma Science*, Vol. 30, No. 4, 2002, pp. 1400–1408.

[18]Haacke, M., Humpert, C., and Pietsch, G. J., "Influence of Field Strength and Energy Distribution of Different Barrier Discharge Arrangements on Ozone Generation," *Ozone Science and Engineering*, Vol. 24, 2002, pp. 193–201.

[19]Mangolini, L., Orlov, K., Kortshagen, U., Heberlein, J., and Kogelschatz, U., "Study of Different Discharge Regimes in a Dielectric Barrier Discharge: Electrical and Optical Characterization," American Physical Society, 55th Annual Gaseous Electronics Conf., Oct. 2002, Paper NR2.003.

[20]Kang, W. S., Kim, Y., and Hong, S. E., "Spatio-Temporal Images of Single Streamer Propagation in Dielectric Barrier Discharge," *IEEE Transactions on Plasma Science*, Vol. 30, No. 1, 2002, pp. 166–167.

[21]Napatovich, A. P., "Overview of Atmospheric Pressure Discharges Producing Nonthermal Plasmas," *Plasmas and Polymers*, Vol. 6, No. 1, 2001, pp. 1–14.

[22]Gherardi, N., and Massines, F., "Mechanisms Controlling the Transition from Glow Silent Discharge to Streamer Discharge in Nitrogen," *IEEE Transactions on Plasma Science*, Vol. 29, No. 3, 2001, pp. 536–544.

[23]Liu, S., and Neiger, M., "Excitation of Dielectric Barrier Discharges by Unipolar Submicrosecond Square Pulses," *Journal of Physics D: Applied Physics*, Vol. 34, No. 11, 2001, pp. 1632–1638.

[24]Kunhardt, E. E., "Generation of Large-Volume, Atmospheric-Pressure, Nonequilibrium Plasmas," *IEEE Transactions on Plasma Science,* Vol. 28, No. 1, 2000, pp. 189–200.

[25]Gibalov, V. I., and Pietsch, G. J., "The Development of Dielectric Barrier Discharges in Gas Gaps and on Surfaces," *Journal of Physics D: Applied Physics*, Vol. 33, No. 20, 2000, pp. 2618–2636.

[26]Steinle, G., Neundorf, D., Hiller, W., and Pietralla, M., "Two-Dimensional Simulation of Filaments in Barrier Discharges," *Journal of Physics D: Applied Physics*, Vol. 32, No. 12, 1999, pp. 1350–1356.

[27]Massines, F., Rabehi, A., Decomps, P., Ben Gadri, R., Segur, P., and Mayoux, C., "Experimental and Theoretical Study of a Glow Discharge at Atmospheric Pressure Controlled by Dielectric Barrier," *Journal of Applied Physics*, Vol. 83, No. 6, 1998, pp. 2950–2957.

[28]Xu, X., and Kushner, M. J., "Multiple Microdischarge Dynamics in Dielectric Barrier Discharges," *Journal of Applied Physics*, Vol. 84, No. 8, 1998, pp. 4153–4160.

[29]Li, J., and Dhali, S. K., "Simulation of Microdischarges in a Dielectric Barrier Discharge," *Journal of Applied Physics*, Vol. 82, No. 9, 1997, pp. 4205–4210.

[30]Falkenstein, Z., and Coogan, J. J., "Microdischarge Behavior in the Silent Discharge of Nitrogen–Oxygen and Water–Air Mixtures," *Journal of Physics D: Applied Physics*, Vol. 30, No. 5, 1997, pp. 817–825.

[31]VanDyken, R. D., Enloe, C. L., and McLaughlin, T. E., "Parametric Investigations of Single Dielectric Barrier Plasma Actuator," AIAA Paper 2004-846, Jan. 2004.

[32]Font, G., "Boundary Layer Control with Atmospheric Plasma Discharges," AIAA Paper 2004-3574, July 2004.

[33]Phelps, A. V., and Pitchford, L. C., JILA Information Center, Rept. 26, Univ. of Colorado, 1985.

[34]Ellis, H. W., Pai, R. Y., McDaniel, E. W., Mason, E. A., and Viehland, L. A., *Atomic Data and Nuclear Data Tables*, Vol. 17, 1976, pp. 177–210.

[35]Knyazev, B. A., Greenly, J. B., Hammer, D. A., Krastelev, E. G., and Cuneo, M. E., "Telescopic Refractive Index Gradient Diagnostic on an Ion Diode Anode Plasma," *Review of Scientific Instruments*, Vol. 72, No. 5, 2001, pp. 2310–2321.

[36]Cuneo, M. E., Lockner, T. R., and Tisone, G. C., "A Refractive INdex Gradient (RING) Diagnostic for Transient Discharges or Expansions of Vapor or Plasmas," *IEEE Transactions on Plasma Science*, Vol. 19, No. 5, 1991, pp. 800–813.

[37]Enloe, C. L., Gilgenbach, R. M., and Meachum, J. S., "Fast, Sensitive Laser Deflection System Suitable for Transient Plasma Analysis," *Review of Scientific Instruments*, Vol. 58, No. 9, 1987, pp. 1597–1600.

[38]Greenspan, M. A., and Reddy, K. V., "A Laser Deflection Technique for Sensitive Measurements of a Reduced-Density Channel in Neutral Gas," *Applied Physics Letters*, Vol. 40, No. 7, 1982, pp. 576–578.

[39]Enloe, C. L., Brake, M. L., and Repetti, T. E., "Laser Deflection Through a Spark," *American Journal of Physics*, Vol. 58, No. 4, 1990, pp. 400–403.

[40]Baird, C., Enloe, C. L., McLaughlin, T. E., Baughn, J. W., "Acoustic Testing of the Dielectric Barrier Discharge (DBD) Plasma Actuator," AIAA Paper 2005-0565, Jan. 2005.

[41]Orlov, D. M., and Corke, T. C., "Numerical Simulation of Aerodynamic Plasma Actuator Effects," AIAA Paper 2005-1083, Jan. 2005.

M. Auweter-Kurtz
Associate Editor